RESEARCH ARTICLE

Variability of breaking wave characteristics and impact loads on offshore wind turbines supported by monopiles

S. Hallowell[1], A. T. Myers[1] and S. R. Arwade[2]

[1] Department of Civil and Environmental Engineering, Northeastern University, Boston, Massachusetts 02215, USA
[2] Department of Civil and Environmental Engineering, University of Massachusetts, Amherst, Massachusetts 01003, USA

ABSTRACT

Most existing and planned offshore wind turbines (OWTs) are located in shallow water where the possibility of breaking waves impacting the structure may influence design. Breaking waves and their associated impact loads are challenging to model because the breaking process is a strongly non-linear phenomenon with significant statistical scattering. Given the challenges and uncertainty in modeling breaking waves, there is a need for comparing existing models with simultaneous environmental and structural measurements taken from utility-scale OWTs exposed to breaking waves. Overall, such measurements are lacking; however, one exception is the Offshore Wind Turbines at Exposed Sites project, which recorded sea state conditions and associated structural loads for a 2.0 MW OWT supported by a monopile and located at the Blyth wind farm off the coast of England. Measurements were recorded over a 17 month campaign between 2001 and 2003, a period that included a storm that exposed the instrumented OWT to dozens of breaking waves. This paper uses the measurements from this campaign to categorize and identify breaking waves and quantify the variability of their impact loads. For this particular site and turbine, the distribution of measured mudline moments due to breaking waves has a mean of 8.7 MN-m, a coefficient of variation of 26% and a maximum of 14.9 MN-m. The accuracy of several breaking wave limits and impact force models is compared with the measurements, and the impact force models are shown to represent the measurements with varying accuracy and to be sensitive to modeling assumptions. Copyright © 2015 John Wiley & Sons, Ltd.

NOMENCLATURE

a_x	local water particle acceleration
C	wave celerity
C_d	drag coefficient in Morison equation
C_m	inertial coefficient in Morison equation
C_s	slam coefficient in Morison equation
d	local water depth
d_z	depth corresponding to individual wave
F_I	inertia force
F_D	drag force
F_s	slam force
F_t	total force
g	gravitational constant
H_b	breaking wave height
H_s	significant wave height
H_z	height of individual wave

k wave parameter
L_b breaking wavelength
L_z wavelength of individual wave
M_f filtered moment response
M_r resultant moment
M_x moment in the x-direction
M_z resultant moment attributed to an individual wave
R radius of monopile
t_s slam duration
T_p peak spectral period
T_z period of individual wave
u local water particle velocity
β_s sea floor slope
η wave elevation profile
ρ density of seawater

1. INTRODUCTION

Offshore wind energy is a vast, largely untapped resource. In the USA alone, the potential resource is estimated at 4150 GW.[1] The US Department of Energy has set a target of generating 54 GW from offshore wind by 2030.[2] Reaching this target will require a significant reduction in the cost of generating energy from offshore wind, which is currently twice the cost of generating energy from traditional carbon-based sources.[3] One factor contributing to the high cost of offshore wind-generated energy is uncertainty in the calculation of structural loads on offshore wind turbine (OWT) support structures under extreme environmental conditions, such as breaking waves. Breaking wave forces can, in some cases, control the design and fragility of an OWT support structure.[4,5] Breaking waves occur when a wave becomes so steep that it becomes unstable, thereby converting a portion of its potential energy to kinetic energy[6] and causing potentially higher drag and inertial forces, referred to as 'slam' or 'impact' forces, when compared with an unbroken wave of identical size.

Of the 318 GW of worldwide offshore wind capacity installed as of 2014, 63% is located in shallow water (water depth <30 m), where, all else being equal, OWTs can be installed less expensively.[7] Of the 4150 GW of potential offshore wind resource available in the USA, 1070 GW is located in shallow water.[1] In shallow water depths, stiffness and strength requirements for OWT support structures are commonly realized with the simplest of support structures, a monopile, which is a circular hollow steel tube that is embedded into the seabed and extends above sea level where it interfaces through a transition piece with the OWT tower. Roughly 66% of the existing worldwide offshore wind capacity is supported by monopiles.[7] While the present economics of OWTs clearly favor shallow water sites and monopile support structures, such conditions are also prone to large lateral forces on the monopile caused by the impact of breaking waves. Such waves are most likely in shallow water, where waves interacting with the seafloor are more likely to become unstable and break.

The most widely used international standard for the design of OWT support structures is International Electrotechnical Commision (IEC) 61400-3.[8] This standard requires a site-specific assessment of whether breaking waves will occur under design conditions, and if so, an estimate of their loads. An assessment of whether a wave will break is based on a breaking wave limit, such as those developed by McCowan (1894), Miche (1944), Goda (1974) or Battjes (2000).[8,9] If a site is found to be susceptible to breaking waves, the IEC standard recommends the calculation of impact loads using the Wienke–Oumerachi model,[10] a simple model that is based on the peak impact pressure developed by Wagner (1932) but with an adjustment to account for the decreasing impact pressure with time, as predicted by the Bernoulli equation and verified with wave flume experiments. Both the breaking wave limits and the estimation of impact loads are based on semi-empirical models developed using wave tank experiments, i.e. scaled experiments that comprised regular waves, controlled bathymetry and scaled structures. For OWTs installed in the field, the conditions are more complex, and this can introduce considerable variability in the characteristics of breaking waves and a significant departure from predicted characteristics based on wave tank experiments.[5] More complicated numerical models and methods for simulating breaking waves also exist (e.g. Schultz et al., 1994; Marino et al., 2011),[11,12] but, it is the authors' understanding that these models are rarely used in design practice. Although there are a variety of methods to simulate breaking waves, the accurate estimation of loads due to breaking waves is a challenging endeavor because breaking waves are a strongly non-linear phenomenon with significant statistical scattering.[5]

Given the challenges and uncertainty in simulating breaking waves and their associated impact forces on monopiles, there is a need for simultaneous environmental and structural measurements taken from utility-scale OWTs installed in the field. Overall, such measurements are lacking; however, one exception is the Offshore Wind Turbines at Exposed Sites (OWTES) project,[13] which monitored and recorded environmental conditions and associated structural loads over a 17

month campaign for a 2.0 MW OWT supported by a 3.5 m diameter monopile installed in 8.0 m of water at the Blyth offshore wind farm off the coast of England. The monitored conditions were recorded at high frequency (40 Hz) and included measurements of the sea surface elevation and bi-directional mudline overturning moments of the support structure as well as other measurements such as support structure torsion, distributed moments along the tower and support structure, hub height wind speeds and directions (recorded at a nearby met-tower) and the operational condition of the turbine. The 17 month campaign included a noteworthy storm on 9 November 2001, that exposed the instrumented OWT to dozens of breaking waves. This dataset is one of the only available sources of response measurements for a utility-scale OWT subjected to breaking waves and provides valuable insight into several aspects of breaking waves, such as the sea state conditions that lead to wave breaking, the response of a utility-scale support structure impacted by breaking waves and the variability of those loads. With the objective of informing design methods for OWT support structures, this paper analyses measurements of sea surface elevations and mudline moments for the Blyth turbine and, based on observations of these measurements, characterizes the variability in breaking wave conditions and forces.

This paper begins by describing the Blyth site and the associated OWTES data campaign. The next section provides background on breaking waves, including a summary of several models for predicting the occurrence of breaking waves and their impact forces and methods for identifying breaking waves using sea state measurements. In the following section, a novel approach for detecting breaking waves using coupled measurements of sea surface elevations and structural response is introduced. Based on the Blyth measurements and breaking wave detection algorithm, results are plotted and discussed, with particular emphasis on the variability of the breaking wave forces revealed by the measurements, and a comparison between measurements and predictions using several breaking wave models. The paper concludes with a summary of the results.

1.1. Description of Blyth offshore wind farm and data campaign

The statistics and observations presented in this paper are based on data obtained as part of the OWTES project over a 17 month campaign from October 2001 to February 2003.[13] During this period, environmental and structural measurements were recorded at the Blyth offshore wind farm, which is located 1 km off the northeastern coast of England. The farm was commissioned in December 2000 and consists of two Vestas V66 2.0 MW turbines (Vestas Wind Systems A/S, Aarhus, Denmark). Specifications for the wind farm and OWTs are provided in Table I.

One of the turbines at Blyth was instrumented with environmental and structural sensors, including radar to record sea surface elevations at a point near the turbine support structure, 16 strain gauges to measure orthogonal moment demands at eight locations along the OWT tower and support structure and anemometers at a nearby meteorological tower to measure wind velocities and directions. Measurements were recorded at 40 Hz intermittently for a period between October 2001 and February 2003.[13] The wave radar system was mounted 1.8 m outboard of the tower at an elevation of 13.7 m above lowest annual tide. Assuming a typical wave celerity of $9.0\,ms^{-1}$, this sensor location suggests that wave measurements and impact are offset by roughly 0.2 s. The local bathymetry at the site is relatively steep with an average slope of around 10% and this, combined with the shallow water depth, causes the extreme sea state to be highly non-linear and to include breaking waves.[13] Of particular interest during the 17 month data campaign is a set of stormy data from 9 November 2001. During this storm, the average hub-height wind speed exceeded $15\,ms^{-1}$ with gusts up to $40\,ms^{-1}$, and the turbine was in the parked and feathered condition, during which structural loads are assumed to be wave-dominated. The storm included dozens of instances of breaking waves impacting the support structure, and measurements during this storm form the basis for all of the observations in this paper.

1.2. Background on breaking waves

Simulation of breaking waves for the design of OWTs is composed of two parts: predicting when a wave will break and then, if it does, predicting the associated slam loads on the OWT support structure. Modeling of the conditions causing

Table I. Specifications of the Blyth offshore wind farm site and turbines.

Distance to shore	1.6 km
Turbine model	Vestas V66
Turbine capacity	2.0 MW
Mean water depth	8.0 m
Hub height	60 m
Monopile diameter	3.5 m
Tower top mass	80,000 kg
First natural frequency/period	0.47 Hz/2.1 s
Second natural frequency/period	3.0 Hz/0.33 s

a wave to break has been studied for more than a century, and there are many breaking wave criteria that are used in practice. All of these criteria are based on a measure of the wave's steepness, i.e. the ratio of a wave's height to its wavelength or local water depth.[14] Four widely used criteria are the height to depth limit proposed by McCowan in 1894, the height to wavelength limit proposed by Miche in 1944, the height to wavelength criteria accounting for seafloor slope proposed by Goda in 1974 and the height to period limit proposed by Battjes in 2000.[8,9] These breaking wave limits are presented in Table II, where H_b is the breaking wave height, d is the local water depth, L_b is the breaking wavelength, β_s is the local seafloor slope, g is acceleration due to gravity and T_z is the wave period.

The Battjes limit, which is the limit suggested in IEC 61400-3 for water depths such as those at Blyth, is similar to the Miche limit, but with an upper limit of wave height equal to the McCowan limit.[8] The Miche, Goda and Battjes limits all converge to the McCowan limit as the water depth approaches 0. Each of the aforementioned criteria provides a simplified parameterization of the conditions leading to a breaking wave; however, in a realistic ocean environment, wave breaking is influenced significantly by local bathymety, currents, wind-surface interaction and other localized effects that can produce large variability in breaking wave conditions.[9] Further studies by Thornton and Guza (1983) and Babanin *et al.* (2001) found that the likelihood of breaking waves occurring in an irregular wave train is highly dependent on local water depth and seafloor slope.[15,16] More advanced models such as smoothed particle hydrodynamics,[17] boundary element methods [12] and Lattice Boltzmann methods[18] exist but, based on the authors' understanding, are not commonly used in practice.

Once a breaking wave limit is established, the impact loads are estimated. Estimation of breaking wave forces on structures is particularly challenging because such forces are transient, non-linear and variable,[5] and because OWTs are relatively flexible structures with dynamic characteristics that can significantly influence impact loads due to breaking waves. Results from controlled laboratory experiments of breaking waves impacting monopiles show significant variability in the magnitude of impact loads.[19,20] In some cases, the ratio of measured forces between two waves with the same height, period and water depth exceeds 2.0.[19] Advanced methods for estimating the impact forces of breaking waves based on computational fluid dynamics exist, e.g. smoothed particle hydrodynamics, boundary element method and Lattice Boltzman methods; however, these are rarely used in practice. Instead, there are several simplified breaking wave force models that have been proposed, most notably by Goda in 1966, Campbell-Wyenberg in 1980, Armand–Cointe in 1986 and Wienke–Oumerachi in 2005 (Table III), where C_s is the slam coefficient, R is the radius of the monopile, C is wave celerity, t is time and t_s is the slam duration.[5] These models consider the breaking wave forces on cylindrical piles as an additional slamming force parameter, F_s, within the well-known Morison equation,[21] which estimates total wave forces F_t in terms of inertial F_I, drag F_D and slam F_S components, which are each dependent on wave kinematics (the horizontal acceleration a_x for F_I, the horizontal velocity u for F_D and the wave celerity C for F_s).

$$F_t = F_I + F_D + F_S$$
$$F_I = C_m \rho \pi R^2 a_x \quad F_D = C_D \rho R u |u| \quad F_S = \rho C_S R C^2$$

Although these models do not consider many complicating factors that influence breaking wave forces, such as non-linear irregular waves, free surface particle velocities and the spatial variation of slam loads, empirical observations

Table II. Common breaking wave criteria.

Breaking wave limit	Numerical condition
McCowan (1894)	$H_b = 0.78d$
Miche (1944)	$H_b = 0.142 L_b \ \tanh\left(\frac{2\pi d}{L_b}\right)$
Goda (1974)	$H_b = 0.17 L_b \left\{1 - \exp\left[-1.5\frac{\pi d}{L_b}\left(1 + 15 \ \tan \ (\beta_s)^{4/3}\right)\right]\right\}$
Battjes (2000)	$H_b = 0.78d \ \tanh\left(\frac{0.14g}{2\pi(0.78d)}T_z^2\right)$

Table III. Common breaking wave impact models.

Breaking wave impact model	Slam duration, t_s	Slam coefficient, C_s
Goda (1966)	$\frac{R}{C}$	$\pi\left(1 - \frac{C}{R}t\right)$
Campbell–Weynberg (1980)	$\frac{2R}{C}$	$5.15\left(\frac{2R}{2R+19Ct} + \frac{0.107Ct}{2R}\right)$
Armand–Cointe (1986)	$\frac{3R}{C}$	$2\pi - \left[4.72 - \ln\left(\frac{C}{R}t\right)\right]\sqrt{\frac{C}{R}t}$
Wienke–Oumerachi[10]	$\frac{13R}{32C}$	$2\pi - 2\sqrt{\frac{C}{R}t}\left(\tanh^{-1}\sqrt{1 - \frac{C}{4R}t}\right)$

during laboratory experiments have been shown to be reasonably approximated by these models.[10] The IEC 61400-3 standard recommends the Wienke–Oumerachi model for designing OWT support structures.[8] An alternative approach, proposed by Stansby *et al.*,[19] is to estimate maximum breaking wave forces by amplifying moments, calculated for non-breaking waves and the Morison equation, by a factor that depends on the depth parameter kd, where k is the wave parameter and d is the water depth. Stansby *et al.* analysed data from dozens of wave tank experiments of rigid cylinders subjected to breaking waves and proposed maximum values for this amplification factor.

Given the complications and uncertainty of modeling breaking waves, there is a clear need to validate the approaches outlined previously with coupled sea surface measurements and response time histories for utility-scale OWTs. To date, there are little data outside of scaled-laboratory tests that include high-frequency structural measurements and sea surface information. Utility-scale validation of breaking wave models requires a method to detect the occurrence of breaking waves based on measurements. While there are many methods for detecting breaking waves from sea state measurements, such as microwave or radar measurements,[22,23] video recordings,[24] buoy accelerometer measurements,[25] surface spectrum analysis[26] or wavelet analysis,[27] each of these methods requires spatially and temporally distributed measurements of the sea state.

The Blyth data campaign recorded temporally distributed data at a single point, and this information alone is insufficient to reconstruct the spatially distributed wave field because wave profiles evolve as the wave travels in space. The authors are unaware of an existing method for detecting breaking waves from a sea surface time history at a point and, in the following section, propose a detection method that combines such measurements with simultaneous structural response measurements.

1.3. Breaking wave detection method

The high-frequency sea surface measurements obtained at the Blyth offshore wind farm were processed using a novel method to detect breaking waves. The development of this method, which uses both measurements of the sea surface and the structural response, was required because the sea surface data only include measurements from a single sensor, which cannot capture the spatial evolution of wave breaking. Existing methods for detecting breaking waves require spatially distributed measurements[25–27] that are capable of capturing the instant of wave instability. For measurements that are not spatially distributed, wave measurements are taken at an instant when either a wave has not broken or has already broken and therefore no longer has characteristics representative of the instant of instability. Because of this, none of the limits in Table II can be applied to detect breaking waves using the Blyth data because these limits are appropriate only at the instant of instability. This is the motivation for including the structural response as an indicator that a wave has broken at or near the structure. It is important to note that all of the data presented in this paper are taken during non-operational conditions, when the OWT rotor is parked with blades feathered. For simplicity, under these conditions, it is assumed that the wind loading is negligible and that measurements of the structural response can be entirely attributed to wave loading.

The breaking wave detection method requires several steps, which are summarized by the flow chart in Figure 1 and described sequentially here. The first step (Figure 1(a)) is to remove any tidal or surge variance in the sea surface data, obtain a zero-mean wave profile and identify individual waves and their associated parameters, such as height and period. This was achieved by subtracting a 1 min moving average from the sea surface data, leaving a zero mean wave profile devoid of any tidal or surge variances. Next, the data are smoothed using a 1 s moving average to remove high-frequency noise from the wave measurements. Using this clean data, individual waves are identified as occurring between two adjacent zero down-crossings. The height of each individual wave H_z is calculated as the crest to trough amplitude of the wave profile, the period T_z is taken as the time between subsequent down-crossings, while the depth corresponding to each wave d_z is taken as the average depth of the sea surface during a 1 min interval centered at the time corresponding to the crest of the wave. The structural response data recorded between the wave's two down-crossings are paired with the wave profile data. The maximum resultant moment recorded between the zero down-crossings of an individual wave M_z is identified and paired with the wave profile's characteristics, resulting in a set of four parameters (H_z, T_z, d_z and M_z) characterizing each wave. This process is indicated schematically in Figure 1(b).

The next step in the method is to use individual wave characteristics H_z, T_z and d_z and the associated moment response time history (Figure 1(c)) to detect breaking waves. The detection process is based on the hypothesis that breaking waves and only breaking waves will cause oscillation of the structure in its second mode. The basis for this hypothesis is that loads caused by breaking and non-breaking waves can be distinguished by their duration, dynamic characteristics and location, with the former being a short impulse load (less than 1 s) at a concentrated location near the free water surface and the latter being a long periodic load (on the order of 10 s) distributed exponentially between the free water surface and the sea floor. All of these distinctions increase the likelihood that the Blyth OWT will respond more in the second mode (3.0 Hz with shape similar to the second mode shape of a prismatic cantilever beam) after a breaking wave than after a non-breaking wave that is more likely to excite only the first mode (0.47 Hz with shape similar to the first mode shape of a prismatic cantilever beam).

Based on this hypothesis, breaking waves are detected by searching for waves that cause the associated mudline moment history to oscillate significantly in the OWT's second natural frequency. The second mode oscillations are found by
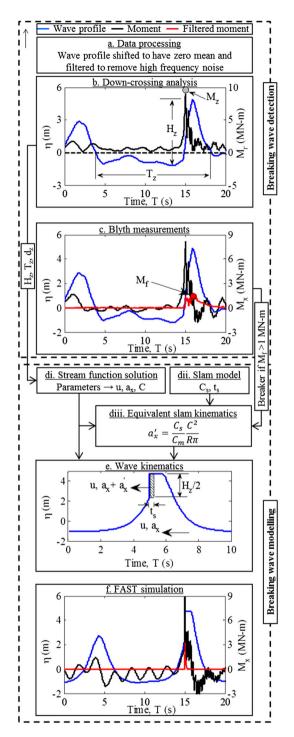
Figure 1. Flow chart showing the process of detecting breaking waves from Blyth measurements and for simulating breaking waves and their loading on OWTs within the analysis program FAST. The process starts with data processing (step a) during which the measured sea surface data are shifted to have zero mean and filtered to remove noise. The next step (step b) is a down-crossing analysis to isolate individual waves and determine the parameters H_z, T_z, d_z and M_z for each wave. The moment response is then filtered (step c) to remove frequency content below that of the second mode and a breaker is detected if the filtered response is greater than 1 MN-m. Wave parameters from step b are used to solve for particle kinematics using Stream function (step di). If breaking waves are detected, a slam model is selected (step dii), and 'equivalent kinematics' is calculated (step diii). The equivalent kinematics is applied to the Stream function wave (step e). The information from step e is then input into a FAST simulation to determine the dynamic response of a model subjected to breaking wave forces. For the particular wave shown in this figure, the outputs from the simulation (step f) are a reasonable approximation of the corresponding measurements (step c).

filtering the moment response time history using a Butterworth filter, implemented using the internal MATLAB [28] function *butter* (MathWorks, Natick, MA, USA) with a stop-band frequency of 2.50 Hz, a pass-band frequency of 2.75 Hz, a stop band attenuation of 4.00 dB and a pass band ripple of 1.00 dB. The filter removes the energy from the response corresponding to lower frequencies, such as those of the first mode of the tower (0.47 Hz) and of the average wave period for extreme sea states (roughly between 0.05 and 0.20 Hz). Since the second fundamental frequency of the structure is 3.0 Hz, any oscillations of the structure at this frequency will pass through the filter, and the resulting response after the filter is applied will have near-zero magnitudes at all times when there is no oscillation at frequencies higher than the first mode. A breaking wave is detected when the maximum of the filtered response time history M_f exceeds a threshold of 1.0 MN-m. The filtering process is indicated schematically in Figure 1(c). The magnitude of the threshold was determined based on an analysis of a dynamic model of the Blyth turbine subjected to a variety of breaking and non-breaking waves.

Estimates of the structural response under the detected breaking waves were made using a dynamic model designed to approximate the most important characteristics of the Blyth turbine and this process is illustrated in Figure 1(d)–(f). The model was created using the National Renewable Energy Laboratory's aeroelastic wind turbine simulation program FAST.[29] The model's characteristics include a fixed-bottom at the mudline, a tower top mass of 80,000 kg, a monopile diameter of 3.5 m, drag and inertial coefficients equal to 0.6 and 1.3 as specified in[13], first and second natural frequencies of 0.47 Hz and 3.0 Hz, distributed stiffness and mass resulting in mode shapes assumed to be similar to those of the Blyth turbine and damping ratios for the first and second mode of 0.5% and 7.5%.[13] Non-linear wave kinematics was approximated using a numerical solution to the Stream function equations of order 30[30] (Figure 1(di)), and breaking wave forces were approximated by converting each of the forces for each of the slam models shown in Table III (Figure 1(dii)) to 'equivalent kinematics' using the Morison equation (Figure 1(diii)). 'Equivalent kinematics' refers to water particle accelerations that induce inertial forces that are equivalent to the slam loads. These accelerations are locally added to the Stream function kinematics during the times appropriate to the particular slam model (Figure 1(e)). The increased kinematics are located based on recommendations in IEC 61400-3, which states that the impact load should be distributed uniformly on the monopile over a length between the top of the breaking wave and the midpoint between the still water level and the top of the breaking wave.[8] The modeled wave kinematics, including 'equivalent kinematics', is then modeled in FAST to estimate the structural response (Figure 1(f)).

Figure 1(c) and (f) respectively shows plots of measured and modeled wave elevations and moment response histories for a breaking wave and a non-breaking wave of similar heights and periods. The key features of the breaking wave detection method are demonstrated in Figure 1(c), which shows the measured response time history of the structure after being impacted by a breaking wave at T = 15 s. The breaking wave parameters found from down-crossing analysis are $H_z = 5.7$ m and $T_z = 12.5$ s. Following the impact of this wave, the mudline moment M_x peaks at 8.1 MN-m, and the structure responds with frequencies close to both the first (0.47 Hz) and second mode (3.0 Hz) of the structure with the higher frequency response decaying quickly (after ~3 s). This observation is reflected by the red line that shows the response M_f after the data have been filtered to remove lower frequency content. The filtered data show a peak reaching 1.4 MN-m following the impact of the breaking wave, which is above the 1.0 MN-m threshold, indicating that this wave would be classified as a breaking wave. At T = ~4 s, the structure is impacted by another wave, with $H_z = 4.8$ m and $T_z = 10$ s. This time, the wave impact causes a much smaller mudline response of 1.7 MN-m, and the filtered response is negligible, indicating that this wave would be classified as a non-breaking wave.

A comparison of Figure 1(c) and (f) shows that the behavior of the structural model reasonably replicates measurements from the Blyth OWT for the two waves shown, specifically the excitation of the second mode of the structure after the impact of a breaking wave and not after the loading of a non-breaking wave with similar characteristics. The peak response to the breaking wave at T = 15 s is simulated as 10.7 MN-m (130% of the measured value) with clear oscillations in the second mode. The filtered modeled response shows a sharp peak of 3.1 MN-m, which is also above the 1.0 MN-m threshold of the breaking wave detection method. The response of the model at T = ~4 s, when the non-breaking wave is modeled, has a peak of 1.4 MN-m (82% of the measured value), and no oscillations are predicted in the second mode. While this specific example is not an exhaustive evaluation of the hypothesis that breaking waves are the lone cause of second mode oscillations of the Blyth structure, the example does show that the hypothesis holds under conditions roughly corresponding to breaking and non-breaking waves acting on the turbines at the Blyth wind farm.

Practically, this method of detection of breaking waves is somewhat limited as it is only useful for a rather specific situation: when structural response measurements are available along with corresponding sea surface measurements that are not spatially distributed. While the latter is often the case for wave measurement recordings at a specific location (e.g. buoy measurements), it is rare to also have simultaneous structural response measurements. Moreover, the method is further limited by the requirement that the structural response is dominated by wave action only. Response time histories that include operational wind loads can cause a structural response in the second mode, which would violate the hypothesis underlying the detection method.

1.4. Evaluation of variability in breaking wave forces and conditions

The Blyth data provide a unique opportunity to assess the variability inherent to breaking wave conditions and impact forces. Figure 2 shows a scatter plot with the wavelength to depth ratio L_z/d_z and the height to depth ratio H_z/d_z of each wave occurring during 3 h of a storm on 9 November 2001, the only event over the entire Blyth campaign during which breaking waves were detected. The measured periods of the individual waves T_z were converted to wavelengths L_z using the linear dispersion relationship for shallow water to allow a direct comparison with the breaking limits in Table II. Spectral representation and statistics ($H_s = 4.7$ m; $T_p = 13.4$ s) for this sea state are provided in Figure 3. In this 3 h period, which includes a total of 1241 waves, 22 breaking waves are detected as having impacted the turbine, resulting in an arrival rate of 7.3 impacts per hour. Five additional breaking waves were detected during the 3 h period before and after the one plotted in Figure 2, resulting in a total of 27 breaking waves detected during the entire Blyth campaign. Each wave on the scatter plot is distinguished as being either breaking, indicated by square markers, or non-breaking, indicated by circle markers. The color of each marker indicates the magnitude of the maximum resultant mudline moment M_z associated with each wave, and it is clear that waves causing maximum moments are neither the highest nor the steepest. For example, the wave causing the maximum measured moment of 14.9 MN-m has an H_z/d and L_z/d of 0.4 and 10, respectively. It is important to remember that the data in Figure 2 are based on the height and steepness of waves measured at a time very near the instant of impact, not at the instant of breaking, because information at the instant of breaking is not discernable from the measurements.
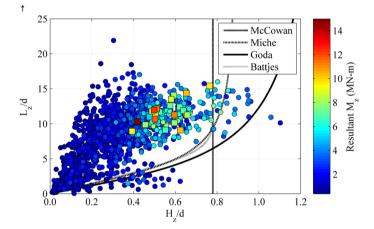

Figure 2. Scatter plot of wavelength to depth ratio L_z/d_z and wave height to depth ratio H_z/d_z for each wave within a 3 h period during a 9 November 2001 storm, with breaking waves represented by square markers and non-breaking waves represented by circle markers. The color of the marker for each wave indicates the magnitude of the resultant moment M_z measured at the Blyth turbine. The four breaking wave conditions in Table III are superimposed on the plots.
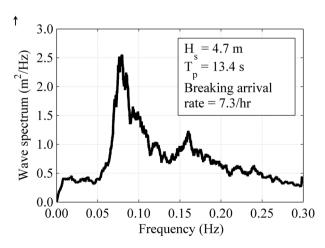

Figure 3. Wave spectra and statistics for 1219 non-breaking and 22 breaking waves measured during the 3 h sea state plotted in Figure 3.

Superimposed in Figure 2 are the McGowan, Miche, Goda and Battjes breaking wave limits. All the waves causing large moments (>9 MN-m) are below these four limits. This plot is useful for identifying false positives of the four breaking wave limits (i.e. waves that did not break but the limits classify as broken) but cannot be used to identify false negatives (i.e. waves that did break but the limits did not classify as broken) because, for the waves detected as having broken, there is no way of knowing the prior values of H_z and L_z at the instant of breaking when the limits are designed to characterize breaking wave conditions. The data in Figure 2 can be decomposed into two types: waves that have not broken and waves that broke at some instant before the measurement. Thus, for both types of data, the breaking wave limits can be interpreted as estimates of the upper bound of H_z and L_z at the instant of impact. The characteristics of all 22 breaking waves, shown in Figure 2, fall on the less steep side of the breaking wave limits. Considering all 22 breaking waves, the mean value and coefficient of variation of H_z/d_z are 0.56 and 15%, the mean value and standard deviation of L_z/d_z are 11.3 and 16% and the correlation coefficient is 0.14.

Based on the 3 h period in Figure 2, the arrival rate for false positives for the McCowan, Miche, Goda and Battjes limits are 9.7, 22, 12 and 24 waves per hour, respectively. The McCowan limit identifies the least false positives since it does not take the relative period or wavelength into consideration, thereby ignoring low height, but high steepness waves. The Battjes limit identifies the most false positives as it is essentially the union between the McCowan and Miche limits. As expected, the Goda limit identifies fewer false positives than Miche, since this limit allows the waves to grow steeper because of the ocean floor slope parameter found in the limit.

The Blyth data also provide useful insight into the variability of impact forces due to breaking waves. Figure 4(a) shows a histogram of measurements of the resultant mudline moment M_z for all 27 breaking waves detected during the entire Blyth campaign. The mean value of M_z for the 27 breaking waves, represented as a vertical solid line in the figure, is
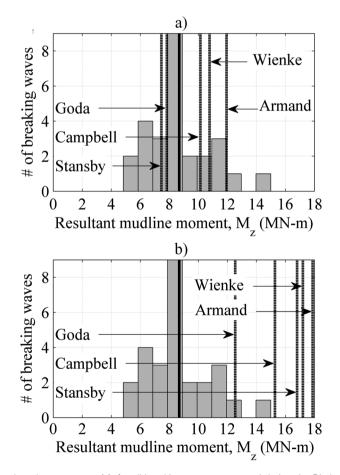

Figure 4. Distributions of resultant base moment M_z for all breaking waves measured during the Blyth campaign. The mean, represented with a solid vertical line, is 8.7 MN-m and the coefficient of variation is 26%. The dotted vertical lines represent moments estimated with each of the four slam models in Table III and the Stansby model for (a) a wave with characteristics at the intersection of the McCowan and Goda breaking wave limits (i.e. $H_z/d_z = 0.78$, $L_z/d_z = 6.5$, kd = 0.97 and Stansby amplification factor of 2.3) and (b) a wave with characteristics at the intersection of the mean value of observations of L_z/d_z for breaking waves at Blyth and the Goda breaking wave limit (i.e. $H_z/d_z = 0.97$, $L_z/d_z = 11.3$, kd = 0.56 and a Stansby amplification factor of 2.7).

8.7 MN-m with a coefficient of variation of 26% and the ratio between the maximum and minimum measurement of M_z is 3.0. There are several explanations for this variability. First, the proposed breaking wave detection method is likely to detect waves that have broken prior to impacting the structure, and the magnitude of the breaking wave impact is known to vary with the location of the onset of breaking relative to the location of the structure.[10,19] Second, at the instant of impact, the dynamic and static conditions of the structure can vary based on factors such as the loading due to prior waves or wind. These varying structural conditions are likely to influence the variability of the impact loads. Third, inherent variability in the shape and kinematics of the breaking wave can cause large variability in the impact loads. The laboratory data presented in Stansby *et al,*[19] which is based on experiments by Luck and Benoit,[20] provide some perspective on the first and third sources of uncertainty. Considering only the data within a range of kd parameter, between 0.9 and 1.0, a range similar to that assumed for waves at the instant of breaking at Blyth, there are 13 measurements of breaking and post-breaking waves impacting a rigid monopile for a range of H_z/d_z (between 0.2 and 0.5) and L_z/d_z (between 6.3 and 6.5). The coefficient of variation of the impact force from these measurements is 32%. Thus, even under the controlled conditions of a laboratory experiment considering a static structure subjected only to a single breaking wave within a relatively tight band of kd, there is similar variability in impact loads from breaking waves as observed in the field.

To assess the performance of the four impact models in Table III and the model proposed by Stansby *et al,*[19] predictions of the impact moment for each model and for wave characteristics on the Goda breaking wave limit are included as five dotted vertical lines in Figure 4(a) and (b). The intent of considering waves with characteristics at the breaking wave limit is to estimate maximum values for the impact moment. The impact moments are calculated at the mudline using the FAST model and the 'equivalent kinematics' procedure described previously and illustrated schematically in Figure 1(d) to (f). Predictions from all five models are calculated for two breaking waves. The first wave (Figure 4(a)) has characteristics at the intersection of the Goda and McCowan breaking wave limits (i.e. $H_z/d_z = 0.78$, $L_z/d_z = 6.5$, kd = 0.97 and Stansby amplification factor of 2.3). The second wave (Figure 4(b)) has characteristics at the intersection of the mean value of observations of L_z/d_z for breaking waves at Blyth and the Goda breaking wave limit (i.e. $H_z/d_z = 0.97$, $L_z/d_z = 11.3$, kd = 0.56 and a Stansby amplification factor of 2.7). Impact forces from the second wave are included to consider the possibility that wave characteristics evolve post-breaking, such that H_z/d_z reduces while L_z/d_z remains constant. For these two waves, the Stream function method does not converge. To model these waves, the authors follow a procedure, proposed by Camp *et al.,*[13] wherein the water depth is scaled up by 40% to achieve convergence and then resulting moments are scaled down by the same percentage. To mimic the dynamic conditions of the Blyth OWT at the instant of impact, the model is subjected to two non-breaking waves prior to the breaking wave. The intent of these two prior waves is to cause realistic structural oscillations at the instant of impact. The two prior waves had heights of 3.8 and 5.2 m and periods of 11.5 and 11.8 s, respectively. These two waves had identical characteristics as the two waves that preceded the wave that caused the maximum impact moment measured during the Blyth campaign. This approach was intended to represent unfavorable structural conditions at the instant of impact. A brief sensitivity study of this approach showed that modeled impact moments vary by as much as 10%, depending on the height of the two waves prior to breaking.

For the first breaking wave (Figure 4(a)), the predictions of mudline moments for the Wienke–Oumeraci, Goda, Armand–Cointe and Campbell–Weynberg models were 10.8, 7.8, 12.0 and 10.2 MN-m, respectively. All of these predicted values are below the maximum measured moment at Blyth. The largest prediction (Armand–Cointe) is 80% of the measured maximum, while the smallest (Goda) is 52% of the measured maximum (14.9 Mn-m). The prediction for the Stansby model (7.5 MN-m) is roughly half of the measured maximum. For the second breaking wave (Figure 4(b)), the predictions from all five models were higher (50–60% higher for the models in Table III and 125% higher for the Stansby model), reflecting the higher celerity and higher wave height of the second breaking wave relative to the first. The predictions of mudline moments for this wave were 17.2, 12.5, 17.9, 15.3 and 16.8 MN-m for the Wienke–Oumeraci, Goda, Armand–Cointe, Campbell–Weynberg and Stansby models, respectively. The predicted values for all of the models, except for the Goda model, are greater (between 2 and 20% greater) than the measured maximum. The large range of the modeled moments (from 7.8 to 12.0 MN-m for the first wave and from 12.5 to 17.9 MN-m for the second wave) is reflective of the sensitivity of breaking wave moments to varying kinematics and their interaction with a dynamic structure. The predictions of the models for the second wave are much closer to the maximum observed moment than the predictions for the first wave. Note that the amplification factors provided by Stansby *et al,* are for estimating maximum impact force and, here, it is assumed that these same factors can be applied to estimate maximum impact mudline moment.

2. CONCLUSIONS

A novel breaking wave detection method, which uses simultaneous point measurements of sea surface elevation and OWT moment response, is introduced. The method is based on the hypothesis that breaking waves, and only breaking waves, will cause oscillations of the Blyth OWT in its second mode. Using this method, 27 breaking waves are detected during one storm that occurred during the 17 month Blyth data measurement campaign. Inspection of the characteristics of these breaking waves showed that the breaking wave limits presented in Table II represent an upper limit on wave steepness with

reasonable accuracy. Analysis of the measurements at the Blyth site showed that breaking waves measured nearly at the moment of impact with an OWT monopile have significantly varying characteristics (measured mean and coefficient of variation of 0.56 and 15% for H_z/d and 11.3 and 16% for L_z/d_z with a correlation coefficient between the two breaking wave parameters of 0.14) and impact loads (measured mean and coefficient of variation of 8.7 MN-m and 26% for the mudline moment) with a maximum of 14.9 MN-m. The maximum moment is caused by a wave with relatively benign characteristics at impact, $H_z/d = 0.4$ and $L_z/d = 10$. The sources of variability in the breaking wave moment measurements can be attributed to the following: variability in the location of the onset of wave breaking relative to the location of the structure, variability in the structural conditions at the instant of impact due to effects such as prior wave loading and wind loading and inherent variability in the shape and kinematics of breaking waves. A comparison with variability in forces observed during controlled laboratory experiments showed that even under controlled conditions and for a tight band of the wave depth parameter kd that is consistent with breaking conditions at Blyth, there is still significant variability (coefficient of variation = 32%) in impact forces.

A method, termed the 'equivalent kinematics' method for including slam forces in the open source simulation program FAST, has been introduced to estimate moments due to breaking waves. The method locally increases kinematics to equivalently represent slam forces within the Morison equation. Using this method, five models for estimating an important design parameter, the maximum breaking wave moment, have been evaluated for two breaking waves: one with characteristics defined by the intersection of the McCowan and Goda breaking wave limits and another defined by the intersection of the Goda limit and L_z/d_z equal to the mean value (11.3) of the observed breaking waves. Compared with measurements at Blyth, the five models performed with varying success. For the first breaking wave, all of the models predicted impact moments less than the maximum measured mudline moment, with the Goda model predicting a moment 52% of the maximum and the Armand–Cointe model predicting a moment 80% of the maximum. For the second breaking wave, the moments predicted by the models were much closer to the observed maximum, with the Goda model predicting 84% of the maximum and the Armand–Cointe model predicting a moment 120% of the maximum. A brief sensitivity study by the authors showed that estimates of breaking wave moments are sensitive to the heights of prior waves.

These results are site and structure-specific, and further investigations of other OWT structures and sites should be undertaken to verify how the findings can be generalized for use in the design of OWT structures. In the absence of such investigations, the authors recommend that monopiles exposed to breaking waves be designed for at least the maximum moment estimated by the five models considered here, for a range of H_z/d_z and L_z/d_z appropriate to breaking conditions at the site, and for unfavorable structural conditions at the instant of impact due to prior wave loading or other sources. Moreover, the authors recommend that offshore design standards provide more specific guidance on the values of H_z/d_z and L_z/d_z to be used for estimation of maximum mudline moments due to breaking waves and on the details of how to embed a breaking wave within an irregular wave train.

ACKNOWLEDGEMENT

REFERENCES

1. Schwartz MN, Heimiller D, Haymes S, Musial W. Assessment of offshore wind energy resources for the United States. National Renewable Energy laboratory, 2010.
2. U.S. Department of Energy. 20% wind energy by 2030: increasing wind energy's contribution to U.S. electricity supply. DOE/GO-102008-2567, 2008.
3. U.S. Energy Information Administration (EIA). Levelized cost of new generation resources in the annual energy outlook 2013. U.S. Department of Energy, 2013.
4. Jha A, Dolan D, Gur T, Soyoz S, Alpdogan C. Comparison of API & IEC standards for offshore wind turbine applications in the US Atlantic Ocean: Phase II. *Contract*, *303*, 2008; 275–3000.
5. Yu Q, Kim K, Lo T-W. Design standards for offshore wind farms. Prepared by American Bureau of Shipping, 2011.
6. Ochi MK, Tsai CH. Prediction of occurrence of breaking waves in deep water. *Journal of Physical Oceanography* 1983; **13**: 2008–20019.
7. Wind Energy Update. Offshore Foundations report extract, 1–16; 2013.
8. International Electrotechnical Commission. IEC 61400-3. Wind turbines—part 3: design requirements for offshore wind turbines, 2009.

9. Jensen MS. Breaking of waves over a steep bottom slope. Aalborg: Hydraulics & Coastal Engineering Laboratory, Department of Civil Engineering, Aalborg University. Series Paper 2004; **22**; 2 ed.

10. Wienke J, Oumeraci H. Breaking wave impact force on a vertical and inclined slender pile—theoretical and large-scale model investigations. *Coastal Engineering* 2005; **52**: 435–462.

11. Schultz WW, Huh J, Griffin OM. Potential energy in steep and breaking waves. *Journal of Fluid Mechanics* 1994; **278**: 201–228.

12. Marino E, Borri C, Lugni C. Influence of wind–waves energy transfer on the impulsive hydrodynamic loads acting on offshore wind turbines. *Journal of Wind Engineering and Industrial Aerodynamics* 2011; **99**: 767–775.

13. Camp TR, Morris MJ, Van Rooij R, Van Der Tempel J, Zaaijer M, Henderson A, Pearce D. Design methods for offshore wind turbines at exposed sites. Final report of the OWTES project, Garrad Hassan and Partners Ltd., Bristol, UK, 2003.

14. Sarpkaya T, Isaacson M. Mechanics of Wave Forces on Offshore Structures. Van Nostrand Reinhold Company: New York, 1981; **96**.

15. Thornton EB, Guza RT. Transformation of wave height distribution. *Journal of Geophysical Research, Oceans* 1983; **88**: 5925–5938.

16. Babanin AV, Young IR, Banner ML. Breaking probabilities for dominant surface waves on water of finite constant depth. *Journal of Geophysical Research, Oceans* 2001; **106**: 11659–11676.

17. Pelfrene J. Study of the SPH method for simulation of regular and breaking waves. *Gent: Universiteit Gent,* 2011.

18. Janssen CF, Grilli ST, Krafczyk M. Modeling of wave breaking and wave-structure interactions by coupling of fully nonlinear potential flow and Lattice-Boltzmann models. In *Proceedings of the Twentieth International Offshore and Polar Engineering Conference Beijing, China,* 2010; 686–693.

19. Stansby PK, Devaney LC, Stallard TJ. Breaking wave loads on monopiles for offshore wind turbines and estimation of extreme overturning moment. *IET Renewable Power Generation* 2013; **7**: 514–420.

20. Luck M, Benoit M. Wave loading on monopile foundation for offshore wind turbines in shallow-water areas. *Int. Conf. Coastal Engineering*. World Scientific Publishing, 2004.

21. Morison JR, Johnson JW, Schaaf SA. The force exerted by surface waves on piles. *Journal of Petroleum Technology* 1950; **2**: 149–154.

22. Phillips OM. On radar returns from the sea surface—Bragg scattering and breaking waves. In *Seventeenth Symposium on Naval Hydrodynamics: Wakes, Free Surface Effects, Boundary Layers and Viscous Flows, Two-phase Flow, Propeller/appendage/hull Interaction,* 1989; 5–15.

23. Jessup AT. Detection and characterization of deep water wave breaking using moderate incidence angle microwave backscatter from the sea surface (No. WHOI-90-27). Woods Hole Oceanographic Institution, MA, 1990.

24. Mironov AS, Dulov VA. Detection of wave breaking using sea surface video records. *Measurement Science and Technology* 2008; **19**: 015405–015415.

25. Pascal RW, Yelland MJ, Srokosz MA, Moat BI, Waugh EM, Comben DH, Comben AG. A spar buoy for high-frequency wave measurements and detection of wave breaking in the open ocean. *Journal of Atmospheric & Oceanic Technology* 2011; **28**: 590–605.

26. Hwang PA. Spectral signature of wave breaking in surface wave components of intermediate-length scale. *Journal of Marine Systems* 2007; **66**: 28–37.

27. Massel SR. Wavelet analysis for processing of ocean surface wave records. *Ocean Engineering* 2001; **28**: 957–987.

28. MATLAB version 8.0.0.783 (R2012b). The MathWorks Inc.: Natick, Massachusetts, 2012.

29. Jonkman JM, Buhl Jr., ML. FAST User's Guide, NREL/EL-500-29798. National Renewable Energy Laboratory: Golden, Colorado, 2005.

30. Fenton JD. The numerical solution of steady water wave problems. *Computers & Geosciences* 1988; **14**: 357–368.